Mircea Popescu

Prediction of the electromagnetic torque in synchronous machines through Maxwell stress harmonic filter (HFT) method

Abstract For the calculation of torque in synchronous motors a local method is analysed, based on the Maxwell stress theory and the filtered contributions due to the harmonics of the magnetic vector potential in the motor air-gap. By considering the space fundamental field only, the method can efficiently estimate the average synchronous torque for a variety or motor topologies, including concentrated winding designs. This approach employs an analytical filter for the Maxwell stress tensor and 'frozen permeability' technique. The proposed method is validated by comparison with FE results for several synchronous motor types: interior permanent magnet motors, wound field motor, synchronous reluctance motor.

Keywords Synchronous machines · Permanent magnet machine · Reluctance machines · Torque ripple · Pulsating torque · Cogging · Finite element method

1 Introduction

The problem of accurate and efficient computation of the torque, based on the results of electromagnetic field finite element analysis (FEA), was widely studied and a large number of numerical procedures have been proposed by other authors, e.g. [1–5]. Most of the techniques are generally applicable to electromagnetic devices and neither exploit the particularities of rotating electrical machines nor provide the kind of insight into the motor parameters and performance, which would directly help with the selections involved in a practical design process.

Synchronous machines exhibit torque ripple components during operation. According to their source the torque ripples can be described as [6]: (a) Cogging torque—only for permanent magnet motors—component generated by the permeance variation as the magnets rotate; this component is measured and computed at open circuit conditions (i.e. with stator currents set to zero); (b) Pulsating torque associated with the interaction of magnetic reluctance variation of the rotor with current MMF's; this component has a significant value only in interior permanent magnet (IPM) machines or salient pole wound field machines and is computed with excitation field (magnets or field currents) set to zero. (c) Pulsating torque associated with the interaction of non-sinusoidal or non-trapezoidal waveform of the induced EMF with current MMF's; this component can estimated directly only when the saturation is ignored.

The aim of the paper is the development of a new computation method to study the design problems for mechanical designs of synchronous motors. These methods are also applicable to conventional designs and are validated using four examples: a brushless AC motor with (IPM) rotor, a wound field synchronous motor and two synchronous reluctance motor with different contents of space MMF harmonics.

The difficulties associated with the precise computation of the electromagnetic torque and its pulsating components from FE solutions have been discussed and some improved procedures proposed [1,3–5,7–10,13,14,17]. The study presented in this paper brings further contributions to the subject, by analyzing the electromagnetic torque with a dedicated formulation [15,16].

2 Theory and mathematical models

2.1 Maxwell stress tensor method [1,2]

Methods based on Maxwell's stress tensor are commonly used in the computation of forces and/or torques for electromagnetic devices when numerical modelling (e.g. finite element method) is employed. The electromagnetic torque is obtained as a surface integral:

$$T_{\mathrm{e}} = \oint_S \mathbf{r} \times \sigma \cdot dS = \oint_S \mathbf{r} \left\{ \frac{\mathbf{1}}{\mu_{\mathbf{0}}} (\mathbf{B} \cdot \mathbf{n}) \mathbf{B} - \frac{1}{2\mu_0} \mathbf{B}^2 \mathbf{n} \right\} dS, \tag{1}$$

where σ is Maxwell's stress tensor and **n** is the unit normal vector of the integration surface.

When Eq. 1 is used for the calculation of the torque of a rotating electrical motor, a closed integration surface that surrounds the rotor in free space must be chosen [1,2]. In a 2D model the surface integral is reduced to a line integral along the air-gap. If a circle of radius r is taken as the integration path, the relation for computing the torque becomes:

$$T_{\mathrm{e}} = \frac{1}{\mu_0} \int_0^{2\pi} r^2 B_{\mathrm{r}} B_\theta \mathrm{d}\theta, \tag{2}$$

where B_r and B_θ are the radial and tangential components of the flux density **B**.

From Eq. 2 it may be noted that only the flux densities on the integration contour are employed, which allows for simple and quick calculation.

If the solutions are exact, the torque value computed with the above expression is independent of the radius r when r varies between the inner and outer radii of the air-gap. However, in an approximate solution (i.e. case of the majority finite element solutions) the integration path has an effect on the result. In practice, the variation of the torque as a function of the radius r may be as high as 50% from the average value, when a typical finite element is used.

If the FEA uses first-order triangular elements, the solution for vector potential **A** is relatively accurate, while the distributions of **B** and **H** are an order less accurate, since these functions are obtained by differentiating the trial functions for **A**. That is, **A** is described by a linear function over each element, but **B** and **H** are piece-wise constant over each element. Important errors can arise in the tangential components of **B** and **H** in elements adjacent to boundaries between materials of different permeabilities (e.g. rotor steel, permanent magnets, air).

For linear (first-order) elements in [1,8] is suggested a zig-zag integration path through the midpoints of the elements and elements sides. Studies [2,7,8] have shown that the integration contour should not be through nodes or along boundaries of elements and that several contours should be chosen to determine an average value and the range of uncertainty for the torque. It is also recommended that the definition of the integration contour to be as displaced several elements (at least two elements) away from any interface boundaries. Even though an integration path has been chosen properly some significant errors can still arise if a coarse mesh is used. Note that Eq. 1 is composed of $\mathbf{B}^2$—this means that stress tensor is one order worse in accuracy than **B**. In the two-dimensional model of an electrical machine, the three-dimensional surface integral in Eq. 1 may be replaced by a volume integral over a hollow shell in free space surrounding the moving rotor. As the true torque is independent of the radius, we obtain by integrating the expression (2) in the radial direction over the air-gap.

$$T_{\mathrm{e}}(r_s - r_r) = \int_{r_r}^{r_s} T_{\mathrm{e}}\, \mathrm{d}r = \frac{1}{\mu_0} \int_{r_r}^{r_s} \left\{ \int_0^{2\pi} r B_r B_\theta \, \mathrm{d}\theta \right\} \mathrm{d}r$$

$$= \frac{1}{\mu_0} \int_{S_{\mathrm{g}}} r B_r B_\theta \, \mathrm{d}S, \tag{3}$$

where r_s and r_r are the outer and inner radii of the air-gap respectively and S_g is the cross sectional area of the air-gap. From the equations above, the torque is obtained sometimes as an integral over the air-gap.

$$T_{\mathrm{e}} = \frac{1}{\mu_0 (r - r_r)} \int_{S_{\mathrm{g}}} r B_r B_\theta \mathrm{d}S. \tag{4}$$

2.2 Maxwell stress harmonic filter (HFT) method [15,16]

A method of improving the accuracy of the Maxwell stress torque computation would be direct derivation of the flux densities components from an analytical expression of the air-gap magnetic vector potential. In cylindrical co-ordinates, which are suitable for radial-flux rotating machines, two concentric circles of radii R_1 and R_2 are defined inside the motor air-gap and used as non-homogenous Dirichlet boundary conditions, with values determined by the magnetic vector potential solution. Inside the cylindrical shell ($R_1 < r < R_2$) the magnetic vector potential can be analytically described as [2] (Fig. 1):

$$A\,(r, \theta) = \sum_{n=1}^{\infty} \Big[\left(c_n r^n + d_n r^{-n} \right) (g_n \cos\,(n\theta) + h_{\,n} \sin\,(n\theta)) \Big]. \tag{5}$$

The magnetic vector potential on the two circular boundaries can be expressed in Fourier series:

$$A(R_1, \theta) = \sum_{n=1}^{\infty} \left[a_{n1} \cos\,(n\theta) + b_{n1} \sin\,(n\theta) \right], \tag{6}$$

$$A(R_2, \theta) = \sum_{n=1}^{\infty} \left[a_{n2} \cos\,(n\theta) + b_{n2} \sin\,(n\theta) \right], \tag{7}$$

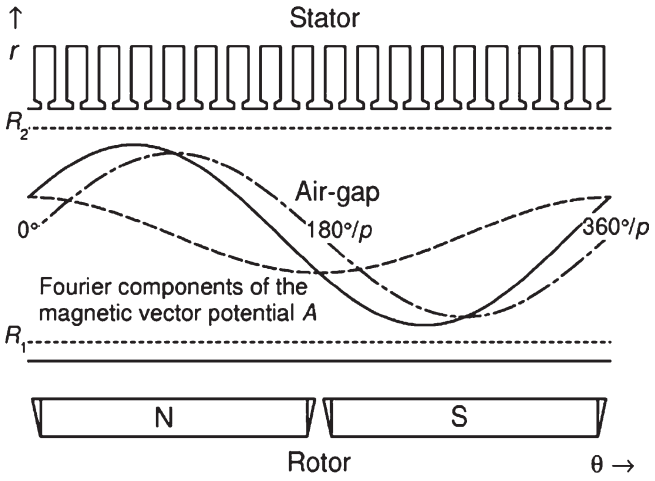

Fig. 1 Explicative for the Maxell HFT method for computing torque based on the harmonics of the vector potential in the motor air-gap

and by writing (7) for R_1 and R_2 the cross products of the coefficients are identified as:

$$c_n g_n = \frac{1}{\delta_n} \cdot \left[a_{n1} \left(\frac{R_1}{R_2} \right)^n - a_{n2} \right], \tag{8}$$

$$c_n h_n = \frac{1}{\delta_n} \cdot \left[b_{n1} \left(\frac{R_1}{R_2} \right)^n - b_{n2} \right], \tag{9}$$

$$d_n g_n = \frac{1}{\delta_n} \cdot \left[a_{n2} - a_{n1} \left(\frac{R_2}{R_1} \right)^n \right], \tag{10}$$

$$d_n h_n = \frac{1}{\delta_n} \cdot \left[b_{n2} - b_{n1} \left(\frac{R_2}{R_1} \right)^n \right], \tag{11}$$

where:

$$\delta_n = \left(\frac{R_1}{R_2} \right)^n - \left(\frac{R_2}{R_1} \right)^n. \tag{12}$$

The magnetic flux density components are calculated by derivation of the magnetic vector potential:

$$B_r = \frac{\partial A}{r\, \partial \theta}; \quad B_\theta = -\frac{\partial A}{\partial r}. \tag{13}$$

Substituting Eqs. 8, 9, 10, 11 and 12 in Eq. 5 and further using Eq. 13 in Eq. 2, a hybrid analytical-numerical computational formula is derived for the electromagnetic torque [15, 16]:

$$T_\mathrm{e} = \left(\frac{P}{2} \right) \cdot \frac{2\,\pi\, \ell_\mathrm{fe}}{\mu_0} \cdot \sum_{n=1}^{\infty} \frac{n^2 (a_{n2} \cdot b_{n1} - a_{n1} \cdot b_{n2})}{\delta_n}. \tag{14}$$

This equation clearly illustrates the proportionality of torque with the motor polarity P and the torque production mechanism by the interaction of the air-gap field harmonics of the same order. Such a formulation is beneficial in identifying and mitigating the source of the parasitic torque harmonics. From a computational point of view, Eq. 14 is advantageous because of its reduced sensitivity to the finite element meshing, especially in the air-gap.

If we associate the coefficients ($a_{n1,2}$) in Eqs. 6 and 7 with the direct d-axis component of each field harmonic and the coefficients ($b_{n1,2}$) in Eqs. 6 and 7 with the quadrature q-axis component of each field harmonic, then the term $n^2(a_{n2} \cdot b_{n1} - a_{n1} \cdot b_{n2})$ in Eq. 14 corresponds to the vectorial product between stator (R_2) and rotor (R_1) field harmonics ($\mathbf{A}_{n1} \otimes \mathbf{A}_{n2}$) of order n. This product is essentially the measure for R times ($\mathbf{B}_{n1} \otimes \mathbf{B}_{n2}$) which is the torque density and where $\mathbf{B}_{n1,2}$ represent the flux-density vectors for rotor and stator nth harmonic fields.

On the other hand, the analytical solution that uses the Fourier series is sensitive to the maximum order of the harmonics considered in the summation [4, 8, 13].

Most notably, this equation illustrates the mechanism of torque production by the interaction of same-order air-gap field harmonics. A certain harmonic will provide a non-zero torque contribution if the sine and/or cosine coefficients of the magnetic vector potential waves on the two boundaries are different, respectively. Physically, this would be caused by a change in the field direction, i.e. a variation of the radial and tangential flux density components, under the provisions of Gauss law of magnetic flux conservation. Other authors [3–5], using different approaches based on the coefficients c_n, d_n, g_n, $h_n \psi$ of Eq. 5, have developed formulae equivalent, in principle, to Eq. 14. This approach can be used in conjunction with any general-purpose electromagnetic FEA software package, also enables insights into the torque components of a synchronous motor.

The method based on Eq. 14, which resembles a harmonic filter and is therefore referred to as Maxwell HFT, has been implemented in the scripting language of a FEA software package [11] and was validated on a number of examples of synchronous motors. In order to enable a fair comparison of new method and classical FEA results, the motors have no rotor-stator axial skew. From a computational point of view, the Maxwell HFT method is advantageous due to its reduced sensitivity to finite element meshing, especially in the air-gap. On the other hand, the Maxwell HFT method is sensitive to parameters such as the maximum order of the harmonics considered for summation. These factors will be further analysed in this paper.

2.3 d-q axis average torque method

The resultant total rotating field under load is determined by both the rotor permanent magnetization and the stator armature currents and has a space fundamental component, which travels at synchronous speed and is responsible for the production of the average torque. The open-circuit flux density high order space harmonics produced by the rotor magnetization also travel at synchronous speed, but their contribution to average torque is zero because their polarity is different to that of the fundamental space harmonic of the armature MMF, which is the only one of the stator harmonics that rotates at synchronous speed. Thus, the Maxwell HFT formulation suggests that a reasonable estimation of the average torque component is obtained by limiting the summation in Eq. 14 to the first electrical harmonic only.

The average torque may be evaluated with the dq formulation:

$$T_\mathrm{e} = \frac{3}{2} \cdot \frac{P}{2} \left(\psi_d i_q - \psi_q i_d \right), \tag{15}$$

where the dq flux linkages $\psi_{d;q}$ and currents $i_{d;q}$ have been determined at each rotor position by applying the Park transformation to the phase quantities.

The comparison of the Maxwell HFT equation Eq. 14, written for the contribution of the fundamental wave only, and of Eq. 15, which is based on the dq theory, points out a similarity in that waveforms placed in quadrature are responsible for torque production. Unlike the dq theory, which identifies the sources of torque as flux linkages and currents, the Maxwell HFT method indicates as the torque source, the spatial shift of the magnetic field harmonics along the air-gap radius. From a theoretical point of view, the dq theory is confined to perfectly sinusoidally distributed windings and excitation.

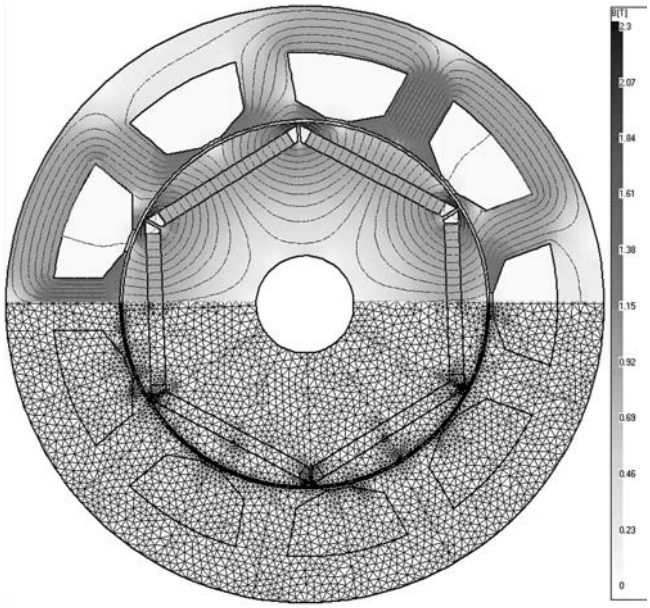

Fig. 2 FE model of a nine-slots six-pole IPM motor design with three-phase concentrated windings

The method of average torque estimation, with the Maxwell HFT equation applied only for the fundamental magnetic vector potential waveform, is remarkable, as it requires only one FE solution at a suitably selected rotor position and current distribution. This can be extremely useful, especially in the early stages of designing a new motor, when computational speed is of essence.

If we assume that the effect of the torque components can be superimposed, a 'frozen permeability' technique can be employed for the segregation of the torque components. The field solution that allows the reluctance torque calculation is obtained with Eq. 14 from an initial field distribution when the motor is under load conditions. The permeability corresponding to each mesh element is 'frozen' and the magnet sources are switched off by setting the flux density to zero. As the employed input permeability describes the saturation conditions in the machine, the computed cogging torque reflects the load conditions. Similarly, the cogging torque can be computed with Eq. 14 if the currents are switched off after computing the permeability for saturation conditions. Finally, by subtracting reluctance and cogging components from the total instantaneous torque the alignment torque my be determined.

This separation of torque components indicates the sources of parasitic torque harmonics and can prove useful in electrical machine design optimization.

2.4 Numerical validation study

The proposed method may be implemented in any scripting language of a FEA software [11]. A numerical validation study was performed by computing the electromagnetic torque of a four three-phase synchronous motors with fractional number of slots/pole:

- Motor A—an IPM motor with nine-slots, six-pole (Fig. 2); magnets material is NdFeB. This motor was selected for the analysis for its high ripple torque content.
- Motor B—a synchronous reluctance motor with nine-slots, six-pole and four layers of low permeability (air) in the rotor (Fig. 3). This motor employs a similar stator with Motor A, but with a much stronger magnetic reluctance variation of the rotor and no excitation or cogging torque.
- Motor C—a wound field salient pole synchronous motor with nine-slots, six-pole (Fig. 4). This motor employs a similar stator with Motor A, but with a much stronger magnetic reluctance variation of the rotor and no cogging torque.
- Motor D—a synchronous reluctance motor with low space MMF harmonics content [12] with 18-slots, four-pole (Fig. 5). This motor was selected for the analysis as it illustrates the presence of ripple torque even when there is no space mmg harmonics effect or cogging torque.

For all motors a 90 Hz fundamental freqency was assumed, i.e. the six-pole motors rotate at 1,800 rpm. The current waveforms are sinusoidal with an amplitude of 100 A and a controll torque angle $\gamma = 30^{\circ}$.

Such motor designs, with a fractional number of slots per pole and phase stator with a distributed winding, are known for their relatively high ripple torque. For the enclosed numerical examples three computations methods have been employed: Maxwell stress method [1], Maxwell stress HFT and virtual work [3]. The Maxwell stress method has been applied using 361 points equidistantly distributed in the air-gap along two circular contours, through the middle of the

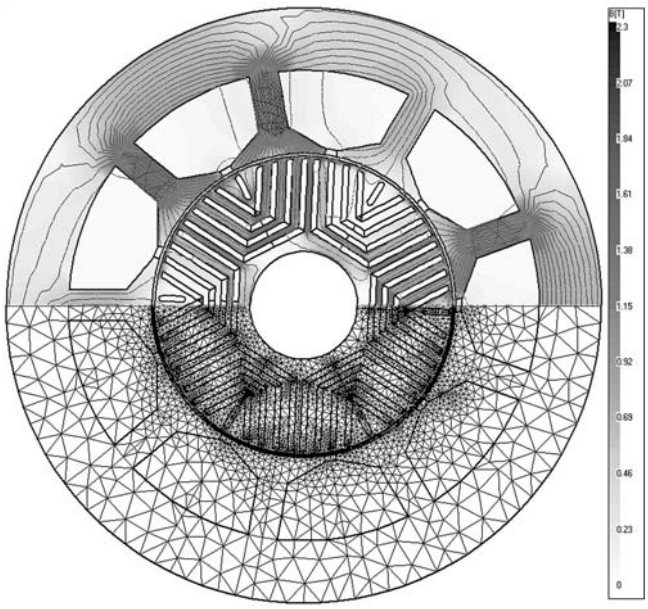

Fig. 3 FE model of a nine-slots six-pole synchronous reluctance motor design with six-phase concentrated windings

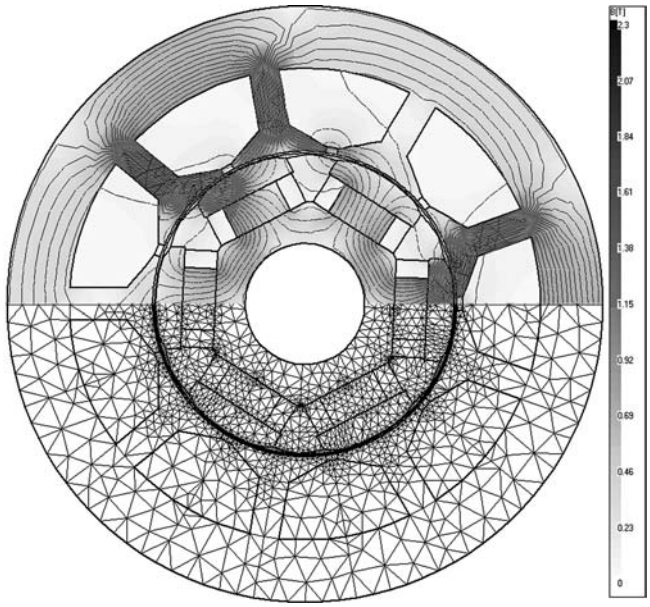

Fig. 4 FE model of a nine-slots six-pole salient pole wound field motor design with six-phase concentrated windings

two central FE layers, respectively. The values reported for the Maxwell stress method were computed by averaging the results for these two contours. For HFT method, the two contours defined the cylindrical shell ($R_1 < r < R_2$) as per Eq. 14 are chosen at the surface of the rotor and stator. Discrete rotor positions have been simulated maintaining the same meshes for the stator and rotor, moving the rotor and re-meshing the air-gap layers.

The comparative graphics between different computation methods from Figs. 6, 8, 10 and 12 illustrate the consistency of HFT method when compared to other methods. The number associated with HFT results in each legend represents the employed harmonics order for the respective case. Note the perfect agreement between the results for all employed methods.

Figures 7, 9, 11 and 13 show a comparison for the average torque estimation between the classical *dq* axis theory and HFT method where only the fundamental harmonic was considered. Motor A (Fig. 7) is the only case in this study when it was necessary to consider up to fifth order field harmonics in order to obtain a reasonable estimation for the average torque.

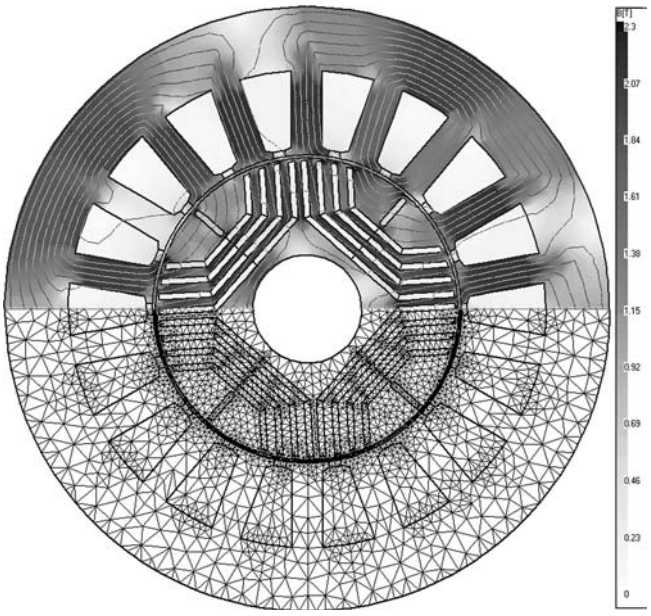

Fig. 5 FE model of a 18-slots four-pole synchronous reluctance motor design with low space harmonics content three-phase windings

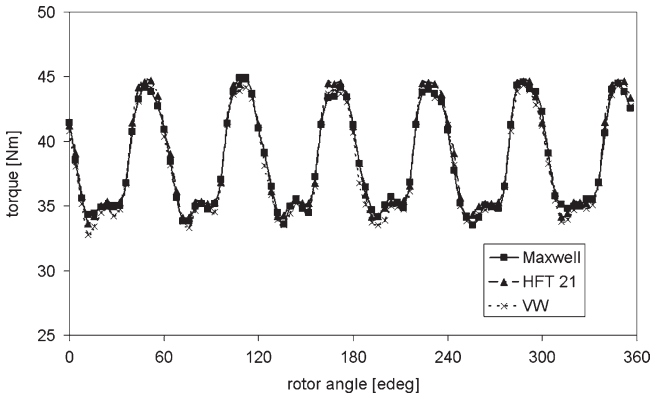

Fig. 6 Torque estimation for a nine slots six-pole IPM motor with three-phase concentrated windings (See Fig. 2)

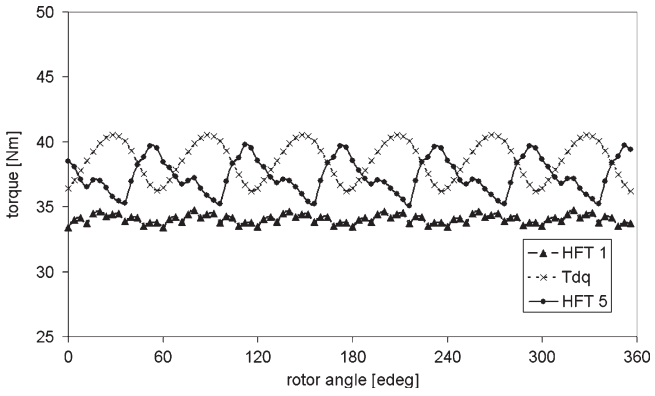

Fig. 7 Average torque estimation using *dq* theory and HFT method for a nine slots six-pole IPM motor with three-phase concentrated windings (See Fig. 2)

Note that as stated in Sect. 2.3, the Maxwell HFT method indicates as the actual torque source, the spatial shift of the magnetic field harmonics along the air-gap radius. Thus, all the ripple torque sources are present in Maxwell HFT method, i.e. cogging torque, space MMF harmonics torque, reluctance torque. Several factors should be considered in the

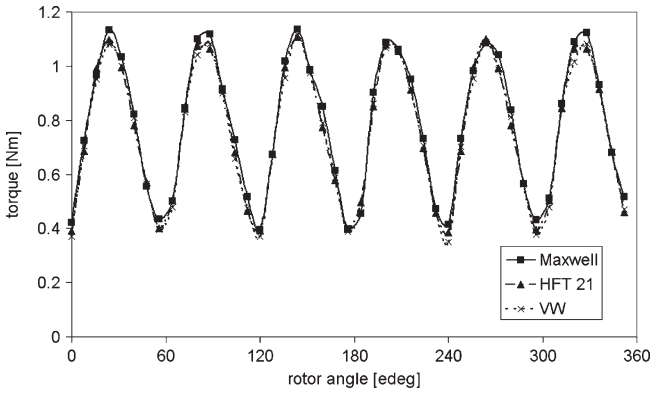

Fig. 8 Torque estimation for a nine slots six-pole synchronous reluctance motor with three-phase concentrated windings (See Fig. 3)

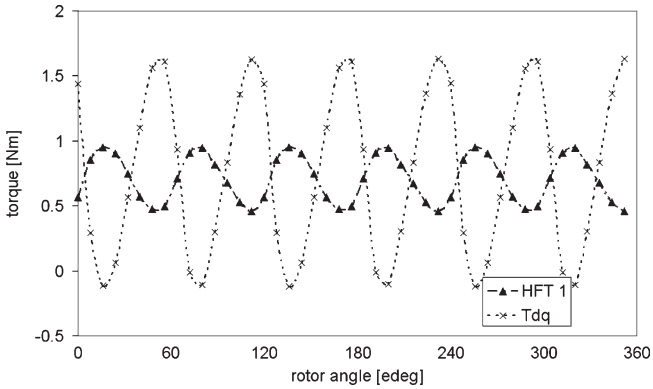

Fig. 9 Average torque estimation using *dq* theory and HFT method for a nine slots six-pole synchronous reluctance motor with three-phase concentrated windings (See Fig. 3)

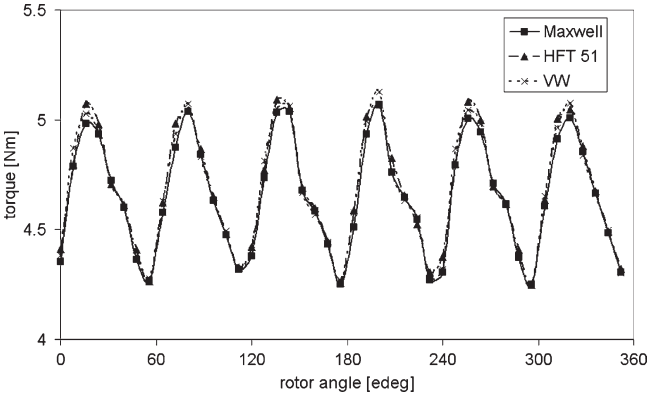

Fig. 10 Torque estimation for a nine slots six-pole salient pole wound field motor with three-phase concentrated windings (See Fig. 4)

explanation of the torque ripple. As the rotor moves, the air-gap permeance varies and the permanent magnet operating point oscillates around an average value, a phenomenon that has been studied for example in [14] in relation with the cogging torque production. As a consequence, the equivalent MMF of the PM and the fundamental air-gap field vary and the rotor positions of zero cogging are more likely to provide the basis for average torque estimation. The motor magnetic circuit is shared by the stator armature field and local saturation can also play a role in the oscillations of the average torque calculations. Of the two types of zero-cogging position, the one corresponding to the alignment of the rotor inter-pole axis with the center of a slot opening not only enjoys a much smaller derivative of the cogging torque but also exhibits a favorable alignment of the stator MMF. Thus, the torque oscillations in Figs. 7, 9, 11 and 13 for HFT method are created by the cogging torque effect.

The average torque estimated with *dq* theory reflects only the interaction between flux-linkages and currents transformed from three-phase system to two phase axis system. It does

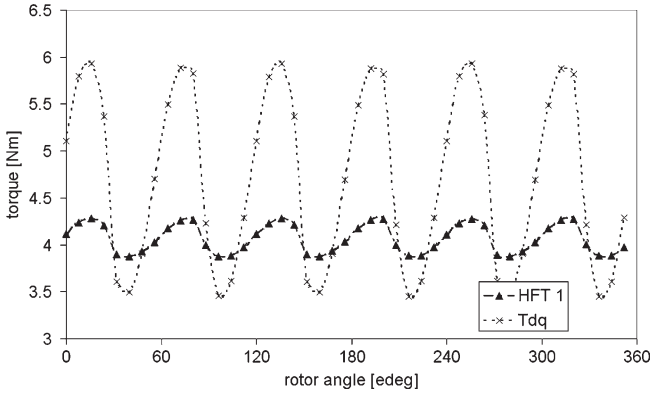

Fig. 11 Average torque estimation using *dq* theory and HFT method for a nine slots six-pole salient pole wound field motor with three-phase concentrated windings (See Fig. 4)

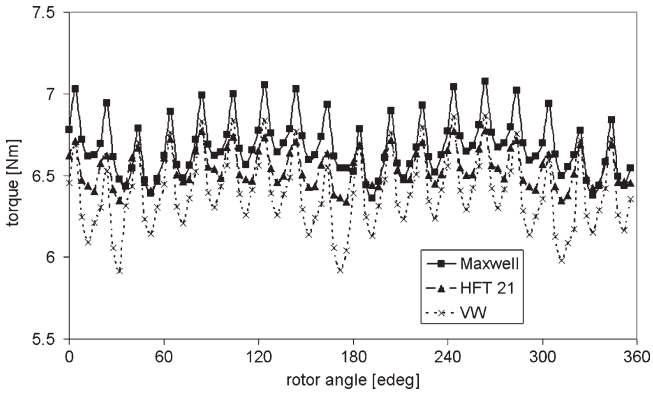

Fig. 12 Torque estimation for a 18 slots four-pole synchronous reluctance motor with low space harmonics content three-phase windings (See Fig. 5)

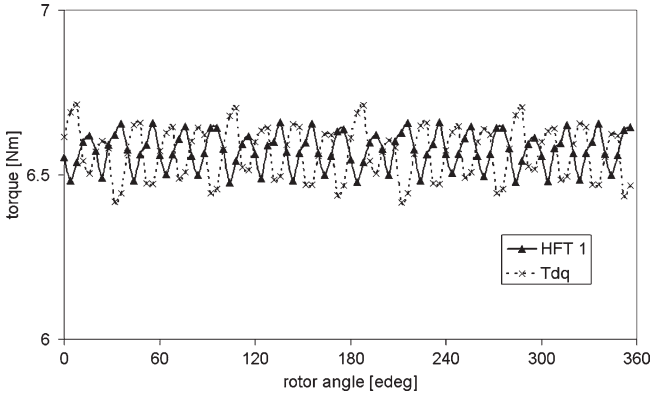

Fig. 13 Average torque estimation using *dq* theory and HFT method for a 18 slots four-pole synchronous reluctance motor with low space harmonics content three-phase windings (See Fig. 5)

not contain any information regarding the ripples created by cogging torque. Thus, for non sinusoidal waveforms of the phase flux-linkages, the *dq* axis average torque will partially reflect the content of space MMF harmonics, but no information on the cogging torque ripples. These differences between the torque computed with HFT method and the torque computed with *dq* axis theory explain the phase shift in their waveforms (See Figs. 7, 9, 11, 13). In some cases these waveforms can be completely in phase opposition (Figs. 7, 9, 13) or they can be in phase (Fig. 11). Note that Fig. 11 corresponds to the case of Motor C—a wound field salient pole synchronous motor, which is the only case with *d* axis inductance (L_d) higher than *q* axis inductance (L_q).

Generally, the numerical results demonstrate that HFT method represent a better solution when the average torque estimation is required, even for a motor that was designed

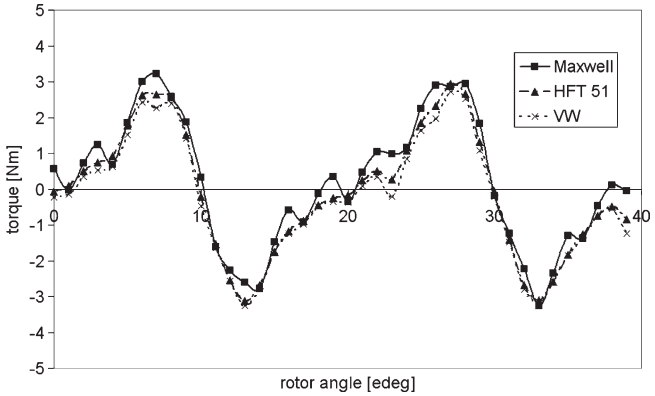

Fig. 14 Cogging torque estimation for a nine slots six-pole IPM motor with three-phase concentrated windings (See Fig. 2)

with a very low space MMF harmonics content (Motor D, Fig. 13).

Different torque components can be estimated in FEA by using 'frozen permeabilities' technique. For example, by switching off the current sources, in Fig. 14 the cogging torque predictions for the Motor A are illustrated. Note the numerical oscillations within Maxwell stress method. This behaviour is consistent with other authors observations [7, 8, 13–17].

3 Conclusions

The numerical and experimental studies performed have indicated that the analytically filtered Maxwell stress method is less sensitive to the variation of computational FE parameters and exhibits reduced numerical noise, as the necessity for the magnetic vector potential numerical differentiation is eliminated. This, together with its apparent improved stability, makes it a recommended choice for sensitive calculations such as instantaneous electromagnetic torque and its components: excitation, reluctance, cogging torque for synchronous motors. Also, this method represents a suitable choice for final design checks and calibration against experimental data.

Acknowledgements The author would like to thank Dr. Dan Ionel who is with AO Smith Corporate Technology Center and Prof. TJE Miller and Mr. M.I. McGilp who are with SPEED Laboratory, University of Glasgow for the technical insights provided and for their contributions in preparing the paper.

References

1. Salon SJ (1995) Finite element analysis of electrical machines, Kluwer Academic Publishers, Boston, ISBN 0-7923-9594-8
2. Binns KJ, Lawrenson PJ, Trowbridge CW (1992) The analytical and numerical solution of electric and magnetic fields. Wiley, Chichester, ISBN 0 471 92460 1
3. Coulomb JL, Meunier G (1984) Finite element implementation of virtual work principle for magnetic or electric force and torque computation. IEEE Trans Magn MAG-20 5:1894–1896
4. Abdel-Razek AA, Coulomb JL, Feliachi M, Sabonnadiere JC (1981) The calculation of electromagnetic torque in saturated electric machines within combined numerical and analytical solutions of the field equations. IEEE Trans Magn MAG-17 6:3250–3522
5. Sadowski N, Lefevre Y, Lajoie-Mazenc M, Cros J (1992) Finite element calculation in electrical machines while considering the movement. IEEE Trans Magn 28(2):1410–1413
6. Jahns TM, Soong WL (1996) Pulsating torque minimization techniques for permanent magnet AC motor — a review. IEEE Trans Ind Electron 43(2):321–330
7. Howe D, Zhu ZQ (1992) The influence of finite element discretisation on the prediction of cogging torque in permanent magnet excited motors. IEEE Trans Magn 28(2):1080–1083
8. Tarnhuvud T, Reichert K (1988) Accuracy problems in force and torque calculation in FE-systems. IEEE Trans Magn 24(1):443–446
9. Hameyer K, Mertens R, Pahner U, Belmans R (1998) New technique to enhance the accuracy of 2-D/3-D field quantities and forces obtained by standard finite-element solutions. IEE Proc Sci. Meas. Technol. 145(2):67–75
10. Marinescu M, Marinescu N (1988) Numerical computation of torques in permanent magnet motors by Maxwell stresss method and energy method. IEEE Trans Magn 24:463–466
11. Miller TJE, McGilp MI (2004) PC-FEA 5.1 for Window – Software. SPEED Laboratory, University of Glasgow, Glasgow
12. Cistelecan M, Demeter E (1999) A new approach of the three phase mono-axial unconventional windings for AC machines. Conf. Rec. of IEMDC , vol 1, pp 323–325
13. Sebastian T, Gangla V (1996) Analysis of induced EMF waveforms and torque ripple in a brushless permanent magnet machine. IEEE Trans Ind Appl 32(1):195–200
14. Dai M, Keyhani A, Sebastian T (2004) Torque ripple of a PM brushless DC motor using finite element method. IEEE Trans Energy Conver 19(1):40–45
15. Popescu M, Ionel DM, Dellinger S, Miller TJE, McGilp MI (2004) Improved finite element computations of torque in brushless permanent magnet motors. In: Conf Rec PEMD 2004 Vol 2. Edinburgh, UK, pp 540–545
16. Ionel DM, Popescu M, Dellinger S, Miller TJE, McGilp MI (2004) Assessment of pulsating torque components in brushless permanent magnet machines through numerical analysis of the electromagnetic field. In: Conf Rec IEEE-IAS 2004, Vol 3. Seattle, USA, pp 1715–1722
17. Parsa L, Hao L, Toliyat H (2002) Optimization of the average and cogging torque in a 3-phase IPM motor drives. In: Conf Rec IEEE IAS Annual Meeting , vol 1. pp 417–424
18. Lee K-S, DeBortoli ML, Lee MJ, Salon SJ (1991) Coupling finite elements and analytical solution in the airgap of electric machines. IEEE Trans Magn 27(5):3955–3957